ELSEVIER

Journal of Nuclear Materials 303 (2002) 125–130

journal of nuclear materials

www.elsevier.com/locate/jnucmat

Investigation of nitric oxide adsorption on Zr(0001)

Y.C. Kang, R.D. Ramsier *

Departments of Physics, Chemistry, and Chemical Engineering, The University of Akron, Akron, OH 44325-4001, USA

Received 11 December 2001; accepted 13 March 2002

Abstract

Nitric oxide (NO, $^{15}N^{18}O$) adsorption on Zr(0001) surfaces is studied by Auger electron spectroscopy (AES), low energy electron diffraction (LEED) and temperature programmed desorption (TPD). The results of our TPD experiments imply that subsurface oxygen and hydrogen are involved in surface reactions during heating, resulting in water and ammonia evolution. NO exposure shifts the Zr(MNV) AES feature by 2 eV indicating a change in oxidation state of +1 after adsorption. A superstructure (1×1) LEED pattern is observed after annealing, and is attributed to residual nitrogen at or near the surface.

PACS: 82.65; 68.10

1. Introduction

Zirconium alloys are subjected to harsh environmental conditions in nuclear applications and their corrosion resistance and durability is well documented. Presently the zirconium materials system is experiencing increased usage in the chemical processing industry where it comes into contact with organics and strong acids and bases [1]. In fact, zirconium and its alloys are one of the few materials systems to exhibit general corrosion resistance in nitric acid (HNO_3) [2] which is used for nuclear fuel reprocessing [3]. Nitrogen implantation has also been shown to alter zirconium alloy corrosion properties [4] and these applications lead us to question the role that nitrogen plays in Zr surface chemistry. In particular, we are interested in how nitrogen influences the reactivity of oxygen and hydrogen present near the surface or in solid solution. Zirconium is well known for its high affinity for hydrogen, oxygen and nitrogen and in the case of oxygen the solubility can be as high as 30% [5]. Studies of such phenomena are crucial to our understanding and control of the chemical nature of zirconium surfaces. In the present paper, we discuss our investigation of nitric oxide (NO) adsorption on Zr(0001) and demonstrate a kinetic isotopic mixing between surface and subsurface species. Nitric oxide is chosen as a model for nitrite and nitrate species present in many applications and the basal plane of Zr is used for comparison with other single crystal studies. Our goal is to use the information reported here to arrive at a mechanistic understanding of Zr surface chemistry.

2. Experimental

An ultrahigh vacuum (UHV) system constructed by this laboratory (base pressure $\sim 1.3 \times 10^{-8}$ Pa) is used in this work. The system consists of three separate chambers isolatable by gate valves; the scanning tunneling microscopy (STM) chamber, a load-locked preparation chamber and the main chamber where most of the analytical tools are housed. These include a combined low energy electron diffraction (LEED) and Auger electron spectroscopy (AES) system, a quadrupole mass spectrometer (QMS) for temperature programmed desorption (TPD), an Ar-ion gun for sample cleaning and an electron flood gun for electron stimulated desorption (ESD) studies. More details about the design and

* Corresponding author. Tel.: +1-330 972 4936; fax: +1-330 972 6918.

E-mail address: rex@uakron.edu (R.D. Ramsier).

0022-3115/02/$ - see front matter
PII: S0022-3115(02)00845-0

operation of this system are available elsewhere [6]. The base pressure is achieved by two sets of pumps. The first set consists of a water-cooled turbomolecular pump backed by a dual stage rotary roughing pump. The second set includes an ion getter pump and a four-filament titanium sublimation pump with a liquid-nitrogen-cooled cold trap.

The Zr(0 0 0 1) single-crystal (1 mm thickness, 6 mm diameter) is in cylindrical disk shape and polished to <0.03 μm surface roughness with an accuracy of orientation better than 1°. The substrate (purchased from Mateck Material–Technologie & Kristalle GmbH) has a guaranteed purity of 99.99% but no chemical analysis or dislocation density data is available. Tantalum wires (0.5 mm diameter, 99.98%, ESPI) are spot welded to the sides of the crystal and mounted on a custom designed sample holder assembly as shown in Fig. 1. The mounting rods are machined from OFHC copper sheet (6.35 mm thickness, 99.99%, ESPI). Two type-E thermocouples (0.25 mm diameter, OMEGA) are spot welded to the sides of the single crystal. The whole assembly is mounted to an x, y, z, θ manipulator. The sample is cooled from a liquid nitrogen reservoir through a pure copper braid and heated resistively by passing direct current via the copper wires (2.03 mm diameter, 99.995%, ESPI) through the Ta mounting wires. The diameters are chosen to maximize the efficiency of heating and cooling the sample and to maintain maneuverability of the sample manipulator. The zirconium surface is cleaned by Ar^+ sputtering (99.9999% purity, Matheson, 2 keV, 2×10^4 μA/m^2) in two-hour cycles followed by annealing to 840 K for 2 min after each cycle.

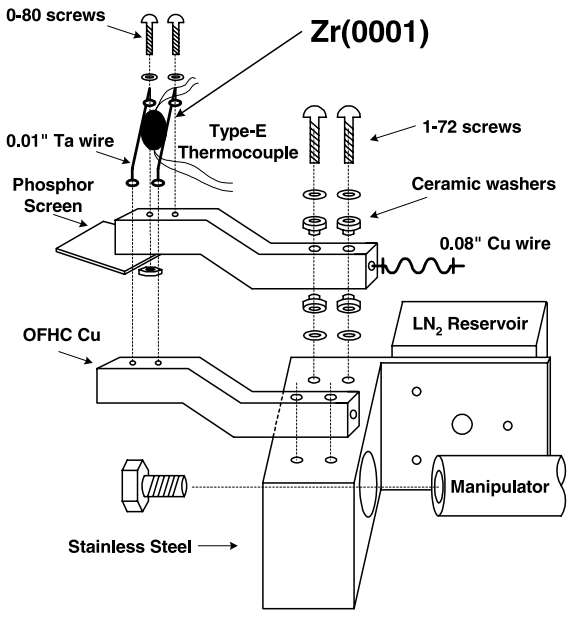

Fig. 1. Schematic diagram of custom designed sample holder assembly.

Lecture bottles of isotope nitric oxide ($^{15}N^{18}O$, min. 99 at.%-^{15}N and min. 95 at.%-^{18}O, Matheson) and nitric oxide (NO, min. 99%, Matheson) are connected to the reactive section of a stainless steel gas handling system for this study. Freeze–pump–thaw cycling and baking of the gas line is performed as needed to maintain the purity of the gases. Sample dosing is performed by backfilling the chamber through precision leak valves and exposure are reported in Langmuir (L) units (1 L = 1.33×10^{-4} Pa s). A QMS is used for TPD and to check the purity of gases. The TPD experiments are performed with a temperature ramp of 1.6 K/s. Electron diffraction data are observed and collected using a digital camera, and exhibit (1×1) patterns characteristic of Zr(0 0 0 1) before NO adsorption. Data from LEED (60–70 eV, 2×10^4 μA/m^2) and AES (3 keV, 1.5×10^5 μA/m^2) are taken after annealing the sample to the desired temperature at a rate of 1.6 K/s followed by cooling back to ~180 K, whereas TPD data are collected during continuous heating.

3. Results

3.1. Temperature programmed desorption

The main products which desorb from Zr(0 0 0 1) after NO exposure are water and ammonia. The complicated kinetics of this system require that we use isotopes to reach a better understanding of the reaction mechanisms. During TPD experiments, we use the multiple ion monitoring mode of the QMS to measure partial pressures of possible combinations of hydrogen, oxygen, and nitrogen atoms, but no significant desorption features are observed except at 20 amu ($H_2{}^{18}O$), 18 amu ($H_2{}^{16}O + {}^{15}NH_3$) and fragments of these. In the model to be discussed in this study, the source of hydrogen is the subsurface region of the Zr sample.

Fig. 2 represents water desorption from Zr(0 0 0 1) after various NO exposures by backfilling at 170 K. The water desorption features are maximized around 650 K. The ratio of desorbed water to ammonia is 12:1 which is calculated by considering the ratios of the QMS cracking fragments of water and ammonia. Figs. 3 and 4 show representative TPD spectra at 20 amu ($H_2{}^{18}O$) and 18 amu ($H_2{}^{16}O + {}^{15}NH_3$) respectively following adsorption of isotopic nitric oxide ($^{15}N^{18}O$) by backfilling at 180 K. The water desorption features are maximized at 610 K, slightly lower than in Fig. 2. This result is similar to the trend observed for ammonia adsorption; a higher adsorption temperature gives a lower desorption temperature [7]. We have developed a model currently in preparation for submission which predicts the direction

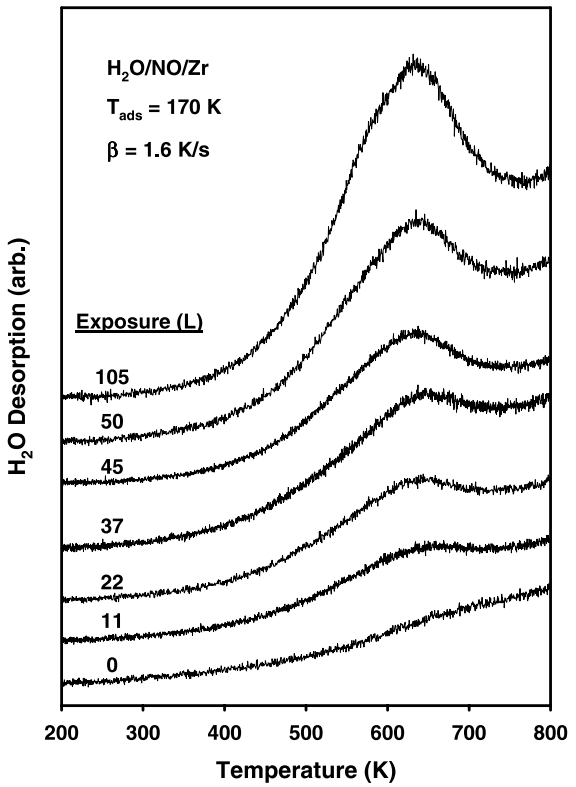

Fig. 2. Representative TPD spectra of $H_2{}^{16}O$ (18 amu) from Zr(0 0 0 1) following 170 K adsorption of NO at various exposures.

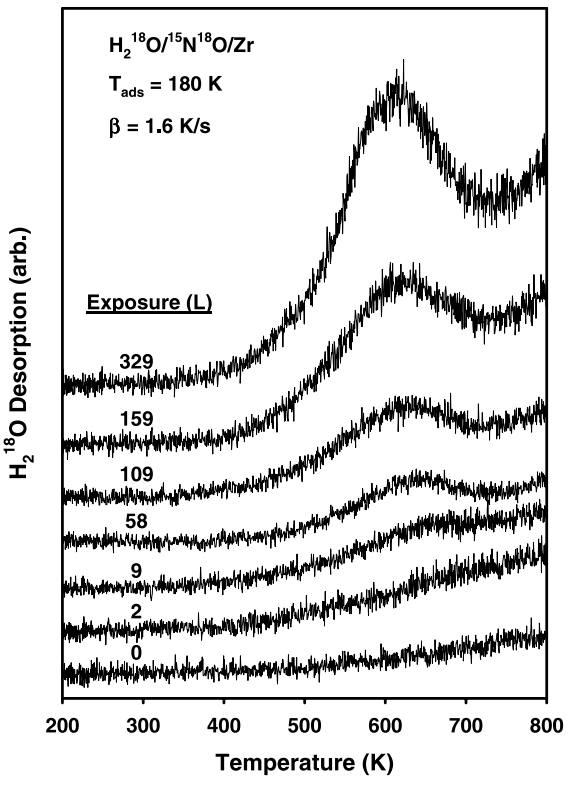

Fig. 3. Representative TPD spectra of $H_2{}^{18}O$ (20 amu) from Zr(0 0 0 1) following 180 K adsorption of $^{15}N^{18}O$ at various exposures.

of this shift in desorption temperatures but not its magnitude. The ratio of isotopic water ($H_2{}^{18}O$) to water ($H_2{}^{16}O$) and ammonia ($^{15}NH_3$) is 1:14:1.3. We assume in our calculation that the ratio of water ($H_2{}^{18}O + H_2{}^{16}O$) to ammonia ($^{15}NH_3$) is the same as the ratio of $H_2{}^{16}O$:$^{14}NH_3$ in the normal nitric oxide experiments of Fig. 2. The relative desorption intensity of $H_2{}^{16}O$ (18 amu) in Fig. 4 is about ten times larger than $H_2{}^{18}O$ in Fig. 3. Oxygen (^{16}O) present in the bulk and subsurface regions apparently participates in surface chemistry on Zr(0 0 0 1).

3.2. Auger electron spectroscopy and low energy electron diffraction

Fig. 5 presents AES spectra of oxidized Zr(0 0 0 1) and the evolution as a function of Ar^+ bombardment. The solid vertical line in the left half of Fig. 5 indicates the Zr(MNV, 147 eV) AES feature. When the sample is fully oxidized, this AES feature is shifted from 147 to 141 eV indicating a stoichiometry close to ZrO_2 [8,9]. The oxygen (KLL, 512 eV) Auger peak-to-peak height (APPH) is intense when the surface is oxidized and the nitrogen (KLL, 379 eV) AES peak is below our detection limit. After Ar^+ cleaning cycles the Zr(MNV) AES feature shifts back to 147 eV and the oxygen APPH decreases; however oxygen is always detectable because of the large solid solubility of O in Zr [8] and the reactive gettering nature of the surface even under UHV conditions.

Fig. 6 shows the AES spectra of NO/Zr(0 0 0 1) taken at various temperatures. When the sample is clean, the Zr(MNV) feature is at 147 eV. After nitric oxide exposure, this feature shifts from 147 to 145 eV, and remains there until heating the sample to 703 K. This result is consistent with a shift of oxidation state by +1 [8,10–12] and could result from mixed stoichiometries of zirconium oxides and nitrides. After annealing the sample to 845 K, the Zr(MNV) feature shifts back to 147 eV. After NO exposure, the APPH of oxygen increases and stays constant until heating the sample to 703 K and then decreases back to the clean surface limit after annealing to 845 K. However, the nitrogen AES feature does not return to the clean surface limit after annealing. In order to recover the clean surface limit with respect to nitrogen, at least four cycles of Ar^+ sputtering are needed.

Fig. 7 presents representative LEED patterns. The left half is the LEED pattern before NO adsorpton, and

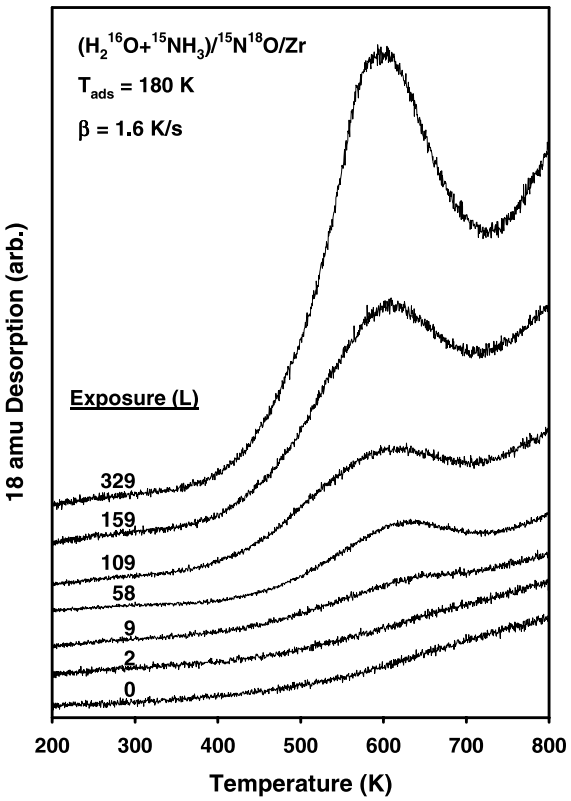

Fig. 4. Representative TPD spectra of 18 amu ($H_2{}^{16}O + {}^{15}NH_3$) from Zr(0 0 0 1) following 180 K adsorption of $^{15}N^{18}O$ at various exposures. (The desorption intensity is about ten times higher than in Fig. 3.)

the right half is taken after NO adsorption and annealing to 703 K followed by cooling the sample to ~180 K. After nitric oxide exposure, the sharp (1×1) LEED pattern becomes diffuse and stays diffuse until heating the sample to 603 K (not shown here). The LEED pattern taken after heating the sample to 703 K is attributed to a superstructure (1×1) nitrogen pattern based on our experience with Zr(0 0 0 1) and the literature [13]. After annealing the sample to 845 K, a clean (1×1) LEED pattern is not recovered easily. In order to recover the clean (1×1) LEED pattern of Zr(0 0 0 1), several cycles of Ar^+ cleaning are needed.

4. Discussion

Surface science studies of nitrogen containing species on zirconium are sparse. One previous study of N_2 and NO adsorption on polycrystalline zirconium at 300 K [14] indicates that N and O atoms diffuse from surface to bulk upon heating and that nitrogen forms an underlayer beneath the surface. Another study of polycrystalline zirconium [15] reports that N_2 adsorption at room temperature leads to the formation of a surface with an electronic density of states similar to that of ZrN. Data from AES indicate that the diffusivity of nitrogen into the bulk is lower than that of oxygen on Zr(0 0 0 1) [13], consistent with results from polycrystalline surfaces [14]. Finally, data from LEED analysis of Zr(0 0 0 1) [13] demonstrate that, following N_2 adsorption, a layer of nitrogen atoms occupies the interstitial octahedral sites between the first two layers of zirconium atoms. These studies imply that atomic nitrogen has a strong affinity for the surface and near-

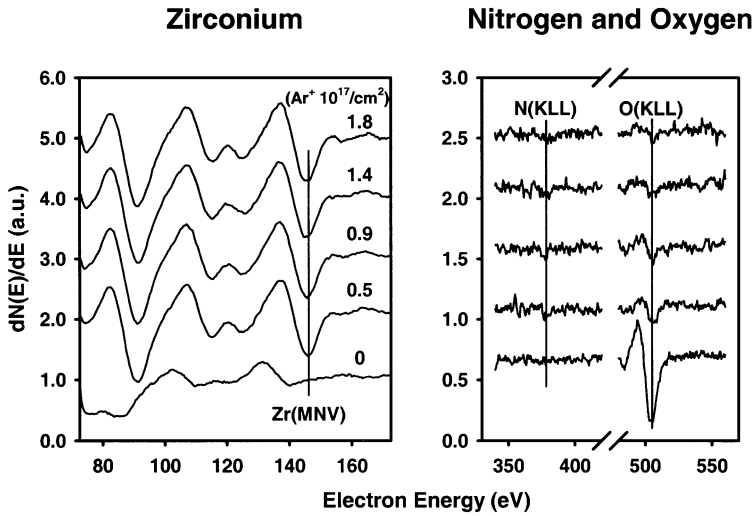

Fig. 5. Auger electron spectra taken after Ar^+ cleaning cycles. The vertical lines indicate the Zr(MNV, 147 eV), N(KLL, 379 eV) and O(KLL, 512 eV) AES features.

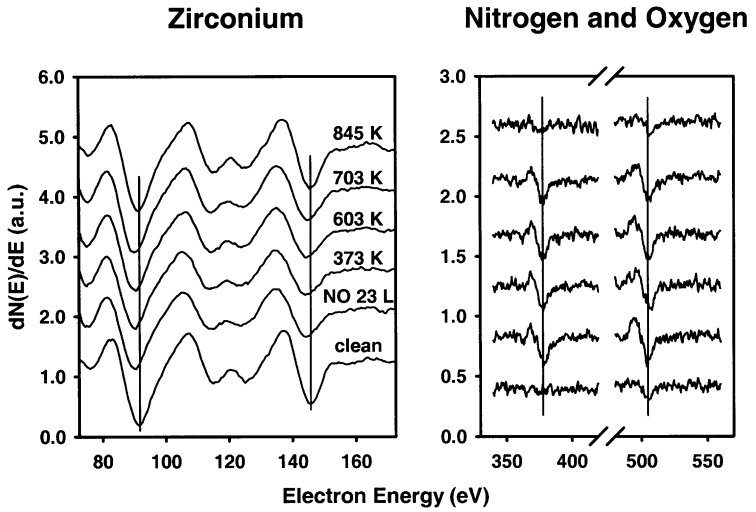

Fig. 6. Auger electron spectra taken after stepwise annealing following 23 L nitric oxide exposure.

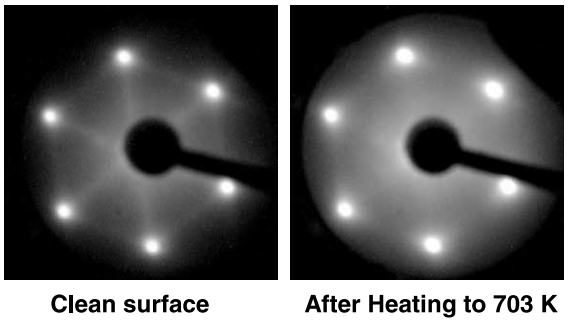

Fig. 7. LEED patterns of Zr(0 0 0 1) surfaces. Left: a clean surface (1×1) LEED pattern. Right: a superstructure (1×1) pattern due to residual nitrogen.

surface regions of zirconium. This is consistent with our AES and LEED findings that following NO adsorption and annealing, residual nitrogen remains at or near the surface of Zr(0 0 0 1).

Surface oxidation of Zr(0 0 0 1) at low coverage occurs layer by layer below room temperature and by the clustering of oxygen atoms into islands after the first two monolayers (ML) at 293 K [10]. Low coverages of oxygen up to 473 K occupy subsurface sites that limit further diffusion of oxygen into the bulk [16]. Tensor LEED studies of 0.5 and 1.0 ML coverages of oxygen on Zr(0 0 0 1) indicate that oxygen resides in the octahedral holes within the first three Zr layers [17,18], and at 2.0 ML coverage in the tetrahedral sites inside the first layer and as an overlayer on the surface [19]. Oxygen induced (2×2) LEED patterns are observed at low coverage ($<$0.5 ML) of oxygen [16–18] and we have observed similar results after heating adsorbed H_2O [6]. However, in the present case where O is adsorbed coincident with N in the form of NO, we do not observe (2×2) LEED superstructures attributable to oxygen. This may indicate that nitrogen is more aggressive than oxygen at occupying the surface and near surface sites.

The behavior of hydrogen adsorbed on Zr(0 0 0 1) is also complex [20–22]. The surface concentration of adsorbed hydrogen atoms depends on the hydrogen gas exposure and thermal history of the sample. High temperature annealing removes surface hydrogen by initiating diffusion into the bulk [20], but the presence of oxygen in the near surface region increases the rate of hydrogen segregation outward [22]. A related study of polycrystalline zirconium indicates that surface oxidation limits subsequent hydrogen adsorption but attracts hydrogen from within the bulk to the surface [14,23–25]. Our observation concerning the formation of water and ammonia during TPD from NO/Zr(0 0 0 1) indicate that this bulk hydrogen is not only kinetically mobile but also chemically reactive.

Our model for water and ammonia production from NO/Zr(0 0 0 1) is summarized by Fig. 8. Dissociative adsorption of nitric oxide occurs followed by mixing of the adsorbed oxygen with subsurface and possibly bulk oxygen. Nitrogen atoms occupy the most energetically favorable sites rather than diffusing into the bulk [13]. When we heat the sample during TPD more nitrogen containing species (NH_3, N_2, NO, etc.) than ^{18}O species ($H_2{}^{18}O$, $^{18}O_2$, $^{16}O^{18}O$, etc.) might be expected because more nitrogen stays near the surface while the ^{18}O dissolves. However, this model is inconsistent with the data since about the same amounts of $^{15}NH_3$ and $H_2{}^{18}O$ desorb during TPD. This is reconciled by data from AES and LEED. Nitrogen atoms still remain near the surface after annealing and a relatively disproportionate

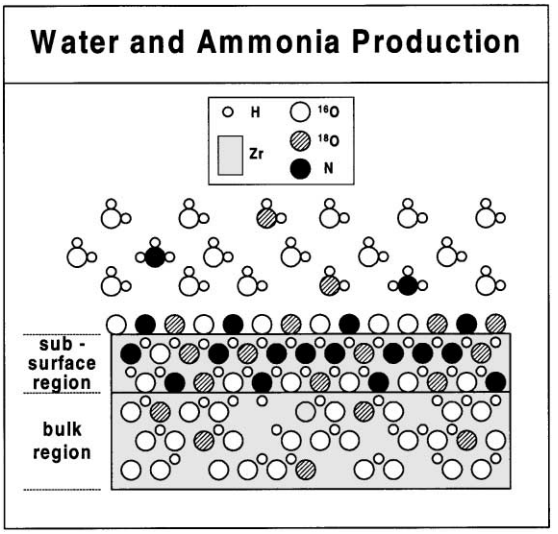

Fig. 8. Illustration of the participation of subsurface and bulk oxygen, nitrogen and hydrogen in water and ammonia production under kinetic conditions.

amount of ^{18}O desorbs. This result implies that a zirconium nitride-like surface is more stable than a zirconium suboxide form. This is consistent with the bond energies of N and O with Zr [26,27], which indicate that Zr–N has a higher bond energy than that of Zr–O. Therefore our data suggest that surface–subsurface transport needs to be considered in the context of Zr surface chemistry, and that nitrogen can play a major role in the resulting reaction kinetics. This information can be used to develop a better understanding of the corrosion resistance and repassivation kinetics of Zr-based materials.

5. Conclusions

In this study, the interaction of Zr(0 0 0 1) with nitric oxide is investigated by AES, LEED and TPD. Data from isotopic TPD experiments show that subsurface oxygen and hydrogen participate in the production of water and ammonia during heating. Our AES data indicate that zirconium is oxidized by +1 after NO adsorption, implying that zirconium oxides, nitrides, or mixed oxynitrides form. A nitrogen induced superstructure (1×1) LEED pattern is observed after annealing, indicating that nitrogen is strongly bound near the surface of Zr(0 0 0 1).

Acknowledgements

Support of this work by Research Corporation is greatly appreciated.

References

[1] B. Cox, in: R.W. Revie (Ed.), Uhlig's Corrosion Handbook, 2nd Ed., Wiley, New York, 2000, Chapter 49.
[2] N.E. Hamner, Corrosion Data Survey, 5th Ed., NACE, 1974.
[3] H. Nagano, H. Kajimura, K. Yamanaka, Mater. Sci. Eng. A 198 (1995) 127.
[4] S.J. Lee, H.S. Kwon, W. Kim, B.H. Choi, Mater. Sci. Eng. A 263 (1999) 23.
[5] T. Tanabe, M. Tanaka, S. Imoto, Surf. Sci. 187 (1987) 499.
[6] Y.C. Kang, M.M. Milovancev, D.A. Clauss, M.A. Lange, R.D. Ramsier, J. Nucl. Mater. 281 (2000) 57.
[7] Y.C. Kang, R.D. Ramsier, Vacuum 64 (2001) 113.
[8] T. Tanabe, M. Tomita, Surf. Sci. 222 (1989) 84.
[9] B. Li, K. Griffiths, C.-S. Zhang, P.R. Norton, Surf. Sci. 370 (1997) 97.
[10] C.-S. Zhang, B.J. Flinn, P.R. Norton, Surf. Sci. 264 (1992) 1.
[11] Y. Nishino, A.R. Krauss, Y. Lin, D.M. Gruen, J. Nucl. Mater. 228 (1996) 346.
[12] M. Tomita, T. Tanabe, S. Imoto, Surf. Sci. 209 (1989) 173.
[13] P.C. Wong, K.A.R. Mitchell, Surf. Sci. 187 (1987) L599.
[14] J.S. Foord, P.J. Goddard, R.M. Lambert, Surf. Sci. 94 (1980) 339.
[15] M. Kurahashi, M. Yamamoto, M. Mabuchi, S. Naito, J. Vac. Sci. Technol. A 15 (1997) 2548.
[16] C.-S. Zhang, B.J. Flinn, I.V. Mitchell, P.R. Norton, Surf. Sci. 245 (1991) 373.
[17] Y.M. Wang, Y.S. Li, K.A.R. Mitchell, Surf. Sci. 342 (1995) 272.
[18] Y.M. Wang, Y.S. Li, K.A.R. Mitchell, Surf. Sci. 343 (1995) L1167.
[19] Y.M. Wang, Y.S. Li, K.A.R. Mitchell, Surf. Sci. 380 (1997) 540.
[20] C.-S. Zhang, B.J. Flinn, K. Griffiths, P.R. Norton, J. Vac. Sci. Technol. A 10 (1992) 2560.
[21] C.-S. Zhang, B.J. Flinn, P.R. Norton, J. Nucl. Mater. 199 (1993) 231.
[22] C.-S. Zhang, B. Li, P.R. Norton, J. Alloys Comp. 231 (1995) 354.
[23] D.A. Asbury, G.B. Hoflund, W.J. Peterson, R.E. Gilbert, R.A. Outlaw, Surf. Sci. 185 (1987) 213.
[24] K. Ojima, K. Ueda, Appl. Surf. Sci. 165 (2000) 149.
[25] K. Ojima, K. Ueda, Appl. Surf. Sci. 165 (2000) 141.
[26] R.I. Masel, Principles of Adsorption and Reaction on Solid Surfaces, Wiley–Interscience, New York, 1996.
[27] M. Yamamoto, M. Kurahashi, C.T. Chan, K.M. Ho, S. Naito, Surf. Sci. 387 (1997) 300.